MIT Open Access Articles

Optimizing the Optoelectronic Properties of Face# On Oriented Poly(3,4#Ethylenedioxythiophene) via Water#Assisted Oxidative Chemical Vapor Deposition

The MIT Faculty has made this article openly available. ***Please share*** how this access benefits you. Your story matters.

Citation	Heydari Gharahcheshmeh, Meysam, Robinson, Maxwell T., Gleason, Edward F. and Gleason, Karen K. 2020. "Optimizing the Optoelectronic Properties of Face#On Oriented Poly(3,4# Ethylenedioxythiophene) via Water#Assisted Oxidative Chemical Vapor Deposition." Advanced Functional Materials, 31 (14).
As Published	http://dx.doi.org/10.1002/adfm.202008712
Publisher	Wiley
Version	Author's final manuscript
Citable link	https://hdl.handle.net/1721.1/140655
Terms of Use	Creative Commons Attribution-Noncommercial-Share Alike
Detailed Terms	http://creativecommons.org/licenses/by-nc-sa/4.0/

Massachusetts Institute of Technology

DSpace@MIT

Check for updates

Optimizing the Optoelectronic Properties of Face-on Oriented Poly(3,4-ethylenedioxythiophene) via Water-Assisted oxidative Chemical Vapor Deposition

Meysam Heydari Gharahcheshmeh[1†], Maxwell T. Robinson[1], Edward F. Gleason[1], Karen K. Gleason[1†]

[1] Department of Chemical Engineering, Massachusetts Institute of Technology, 77 Massachusetts Avenue, Cambridge, MA 02139, United States

[†] Corresponding Authors-Email: mheydari@mit.edu (M.H.), kkgleasn@mit.edu (K.K.G.)

Author Manuscript

Abstract

Engineering the texture and nanostructure to improve the electrical conductivity of semicrystalline conjugated polymers must address the rate-limiting step for charge carrier transport. In highly face-on orientation, the charge transport between chains within a crystallite becomes rate-limiting, which is highly sensitive to the π-π stacking distance and interchain charge transfer integral. Here, face-on oriented semi-crystalline poly(3,4-ethylenedioxythiophene) (PEDOT) thin films were grown via water-assisted (W-A) oxidative chemical vapor deposition (oCVD). Combining W-A with the volatile oxidant, antimony pentachloride ($SbCl_5$), yields an optimized electrical conductivity of 7520 ± 240 S/cm, a record for PEDOT thin films. Systematic control of π-π stacking distance from 3.50 Å down to 3.43 Å yields an electrical conductivity enhancement of ~1,140%. The highest electrical conductivity also corresponds to minimum in Urbach energy of 205 meV, indicating superior morphological order. The figure of merit for transparent conductors, σ_{dc}/σ_{op}, reaches a maximum value of 94, which is 1.9× and 6.7× higher than oCVD PEDOT grown without W-A and utilizing vanadium oxytrichloride ($VOCl_3$) and iron chloride ($FeCl_3$) oxidizing agents, respectively. The W-A oCVD is single-step all-dry process and provides conformal coverage, allowing direct growth on mechanical flexible, rough, and structured surfaces without the need for complex and costly transfer steps.

This is the author manuscript accepted for publication and has undergone full peer review but has not been through the copyediting, typesetting, pagination and proofreading process, which may lead to differences between this version and the Version of Record. Please cite this article as doi: 10.1002/adfm.202008712.

This article is protected by copyright. All rights reserved.

Keywords: PEDOT, oCVD, $SbCl_5$ oxidant, water-assisted growth, π-π stacking distance

1. Introduction

Conjugated polymers hold exceptional promises in a variety of technological applications, including optoelectronics, energy storage, wearable electronics, and biomedical devices.[1,2] Poly(3,4-ethylenedioxythiophene) (PEDOT) has emerged as one of the most researched and promising conjugated polymers for organic electronics.[1–5] The combination of its optical transparency with electrical conductivity (σ), makes PEDOT a mechanically flexible alternative to transparent conductive oxides (TCOs). While providing excellent optoelectronic performance, TCOs, such as indium tin oxide (ITO), suffer from brittleness, raw material scarcity, and high cost.[6,7]

PEDOT is often spin-coated with polystyrene sulfonate (PSS) to form PEDOT:PSS,[8,9] but PEDOT thin films can also be fabricated by electropolymerization,[10,11] in-situ chemical polymerization,[12–15] vapor phase polymerization (VPP),[16–19] and oxidative chemical vapor deposition (oCVD).[20–26] For PEDOT, the highest value of σ to date, 8797 ±1178 S/cm, was reported by Cho et al.[27] in single-crystal nanowires grown by VPP at 50 ˚C using $FeCl_3$ as the oxidant. The nanowire cross-sectional dimensions, 95 nm by 100 nm, likely give pseudo one-dimensional (1D) conductivity.[27] For thin films, which are used in most device applications, conductivity will occur in 2D or 3D,[28] and thus have inherently less efficient charge transport than 1D geometries.[1,6,7] The highest σ for a PEDOT thin film, 6259 ±1468 S/cm, was achieved for a face-on textured oCVD film, 10 nm-thick, displaying 2D conductivity.[29]

The solvent-free oCVD process operates at moderate substrates temperatures and can be scale-up to large areas.[2,30] Using oCVD, PEDOT has been directly deposited onto numerous substrates including silicon and glass;[7,29] papers and plastics;[31] and even the leaves of plants.[32] In the current work, the oCVD growth temperature is limited to 140 ˚C and no post-deposition rinsing is employed, conditions which will facilitate integration with temperature-sensitive and solvent-sensitive substrates. In contrast, materials deposited at high temperature, such as graphene, cannot be directly deposited

This article is protected by copyright. All rights reserved.

Author Manuscript

onto temperature sensitive substrates and devices, and thus their integration relies on complex and costly-transfer steps.[1,33]

Process parameters profoundly affect the texture and nanostructure of semicrystalline oCVD PEDOT thin films, as shown schematically in **Figure 1**. For oCVD, the oxidant saturation ratio (OSR) determines the concentration of oxidant adsorbed on the growth surface and hence the kinetics of oxidative surface reactions. The OSR stands for the ratio of P/P_{sat}, which is the oxidant's partial pressure to its saturation pressure at the temperature of growth. Previously, varying the OSR of the oxidant $VOCl_3$ allowed control of the texture in oCVD PEDOT thin films.[7] The presence of highly face-on texture (Figure 1b) lowers the barrier to intercrystallite charge transport and hence enhances in-plane conductivity.[1,6,7,29] The formation of highly face-on texture may be favored by chain reorientation at deposition temperatures above the glass transition (T_g) for PEDOT (ca. ~100 °C).[1,7] As shown schematically in Figure 1b, a mixture of face-on and edge-on orientation deteriorates the percolation pathway for charge transport, hence lowering σ.[6,7]

Interchain coupling induces a delocalization of charge carriers and is desirable for the enhancement of σ.[6] The interchain charge transfer integral ($t_\perp$) increases as the distance between individual chains (x) decreases and is expressed as:

$$t_\perp = t_0 \exp(-\gamma x) \qquad (1)$$

where t_0 is the charge transfer integral at the minimum distance, and $1/\gamma$ is the wave function overlap decay length.[1,6,7] The carrier mobility is proportional to the square of the inter-chain transfer integral.[6,7,34] In PEDOT, lowering x corresponds to decreasing the π-π stacking distance. The presence of tie-chains between crystallites[1,6,7] and a high degree of backbone planarity[6,9,35,36] can also influence σ in conjugated polymers such as PEDOT. While other factors can vary, such as the crystallite size, chain length, and degree of disorder in the amorphous phase, when a clear correlation of σ exists with the π-π stacking distance, interchain charge transport is likely to be the rate-limiting process.[1,6] The limit of interchain charge transport was previously reported for face-on textured semicrystalline oCVD PEDOT thins films having systematically tunable π-π stacking distances.[7]

This article is protected by copyright. All rights reserved.

Author Manuscript

Herein, sub-nanometer scale control over the π-π stacking distances correlates with the optimization of σ for PEDOT thin films grown by water-assisted (W-A) oCVD. The use of W-A growth for oCVD was motivated by water's ability to act as a proton scavenger, which is anticipated to yield enhanced decomposition of oxidant. Previously, W-A CVD has produced monolayer graphene films with fewer structural defects[37] and uniform graphene/carbon nanotubes (CNTs) structures, as opposed to multi-walled CNTs.[38] Optimizing W-A through variation of the OSR for the volatile oxidant, antimony pentachloride ($SbCl_5$), yielded a record σ of 7520 ± 240 S/cm PEDOT thin films, as a consequence of reducing the π-π stacking distance from 3.50 Å down to 3.43 Å. The maximum σ_{dc}/σ_{op} of ~ 94 represents improvements of 1.9× and 6.7× over the values obtained by oCVD without W-A and with $VOCl_3$ and $FeCl_3$ as the oxidizing agents, respectively. This work not only opens up frontiers for tuning PEDOT thin films using a critical process parameter of OSR and W-A but also provides exciting opportunities for direct integration of high quality as-deposited PEDOT thin films in advanced applications without post-treatment acidic rising steps.

Author Manuscript

This article is protected by copyright. All rights reserved.

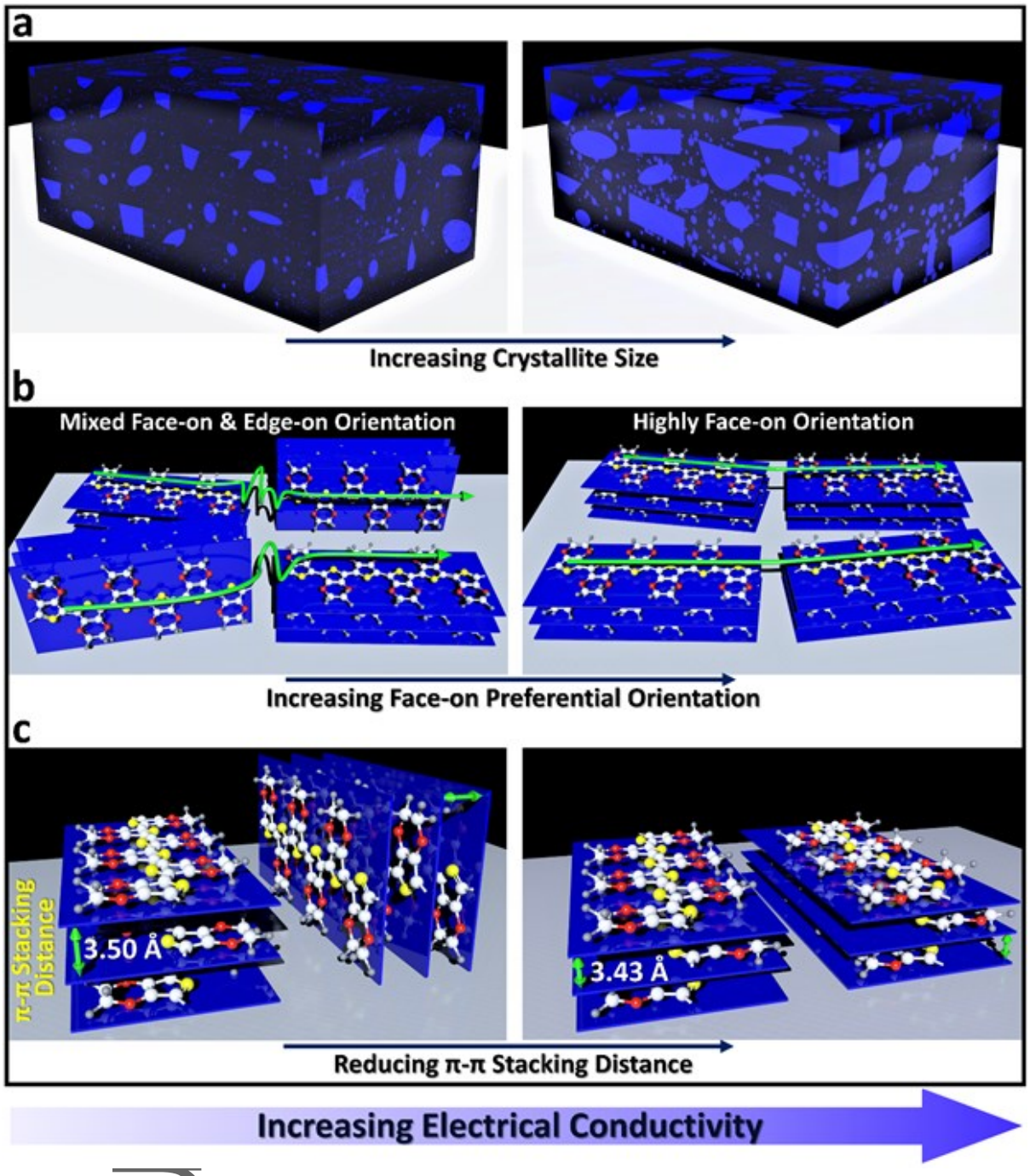

Figure 1. Impacts of W-A growth and OSR on the texture and nanostructure of PEDOT. a) Larger crystallite size of PEDOT thin films is archivable using W-A growth. b) Mixed orientation of face-on and edge-on orientation can be transferred to highly face-on orientation (more desirable orientation for enhancing the in-plane electrical conductivity) by reducing OSR of $SbCl_5$ oxidant and using W-A growth. In both face-on and edge-on orientations, the conjugated backbone is parallel to the substrate plane. However, the π-π stacking direction is parallel and perpendicular to the substrate plane in edge-on and face-on orientation, respectively. c) π-π stacking distance (half of b-axis lattice parameter) of

This article is protected by copyright. All rights reserved.

polymer chains reduces as a consequence of decreasing OSR and using W-A growth. Large crystallite size, highly face-on orientation, and lowering the π-π stacking distance are of great importance for achieving PEDOT with high electrical conductivity.

Author Manuscript

2. Results and Discussion

PEDOT thin films were grown by simultaneously introducing vapors of liquid oxidant ($SbCl_5$), monomer (3,4-ethylenedioxythiophene (EDOT)), and water to the oCVD reactor (**Figure 2**a). The oxidant vapor provides both in-situ doping and oxidative step-growth.[1,2,39] The oCVD PEDOT films were prepared at the modest growth temperatures of either 90 °C or 140 °C with different OSR values. These modest growth temperatures are of interest for directly depositing the oCVD films on mechanically flexible plastic substrates. The detailed protocols for simultaneous introducing the vapors of reactants into the reactor and determining the equilibrium surface concentration of the reactant species are provided in Table S1 (Supporting Information).

An increase in film thickness, and thus deposition rate, was noted both for increasing the OSR and lowering the growth temperature (Figure S1 and Table S2, Supporting Information). The deposition rate increases (from 0.45 to 3.75 nm/min) with an increase in the $SbCl_5$ saturation ratio (from 330 to 1980 ppm) at the surface deposition temperature of 90 °C. At the growth temperature of 140 °C by increasing the $SbCl_5$ saturation ratio from 50 to 290 ppm, the deposition rate rises from 0.17 to 1.37 nm/min. The deposition rate is slightly lower in the case of using water-assisted at both growth temperatures than deposition without using water vapor at the same OSR. Film thicknesses ranged from 10 to 150 nm. Experimental variation of the OSR was facilitated by the similar vapor pressures of $SbCl_5$ oxidant and EDOT monomer. Control of OSR is more difficult for the highly volatile liquid oxidant, $VOCl_3$ (P_{sat}=17.8 Torr at 25 ˚C),[7,40] or the low volatility solid oxidant, $FeCl_3$ (P_{sat}=1 Torr at 194 ˚C, and negligible at 25 ˚C).[5,29,41,42] The $SbCl_5$ oxidant is a liquid of moderate volatility at ambient temperature (P_{sat}=1.2 Torr at 25 ˚C)[42] and can be readily introduced into the oCVD reactor

This article is protected by copyright. All rights reserved.

(Figure 1a). Additionally, $SbCl_5$ has a vapor pressure close to that of the EDOT monomer (P_{sat}=0.278 Torr at 25 ˚C)[42]. The similar vapor pressure of reactants allows easy control of the process parameters, especially the flow rate of reactants at a different working pressure of reactor. However, if there is a large difference between the vapor pressure of reactants, it is generally challenging to achieve sufficient flow of a less reactant species to the reactor. Previously, $SbCl_5$ oxidant was used in the oCVD method for the growth of PEDOT[3] and polythiophene[43], and resulted conducting polymers were integrated into electrodes for redox reactions and supercapacitors, respectively.

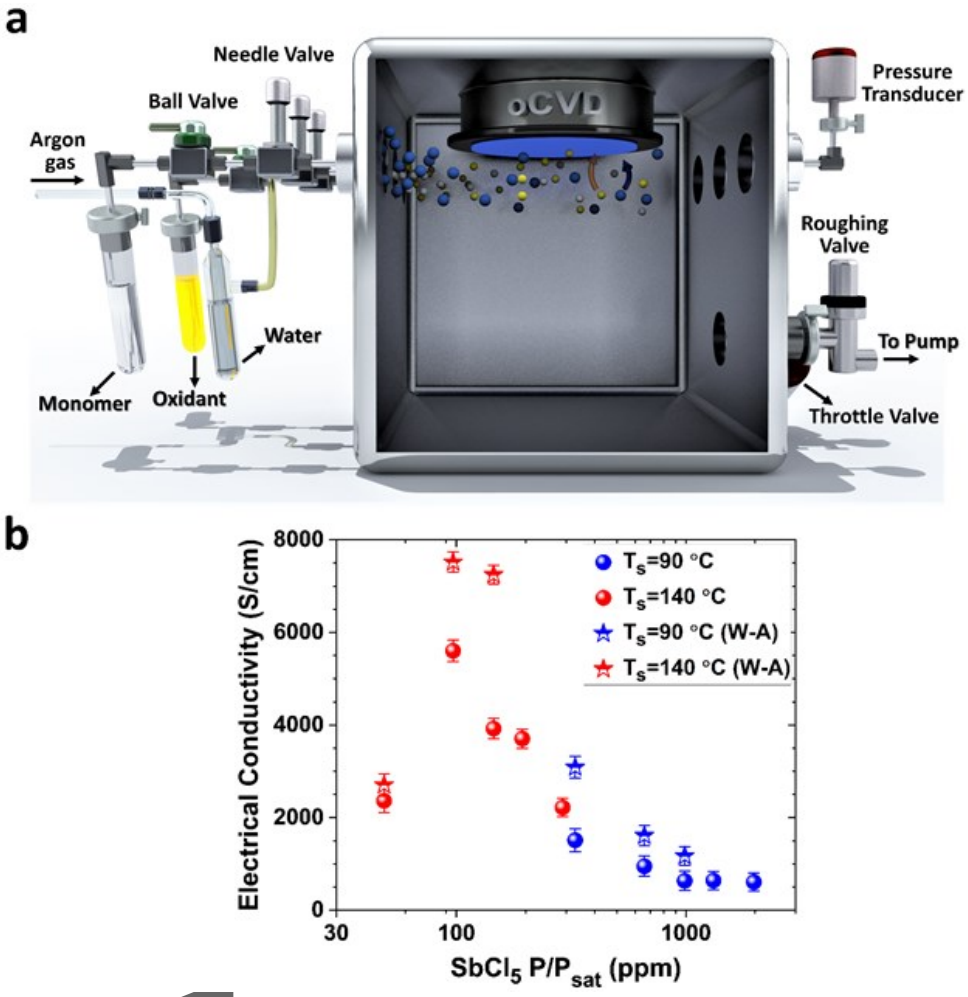

Figure 2. Influence of $SbCl_5$ saturation ratio on the electrical conductivity. a) Schematic illustration of the oCVD reactor using W-A growth. Deionized water vapor, along with the vaporized EDOT and $SbCl_5$ introduced to the reactor. b) Electrical conductivity changes versus $SbCl_5$ saturation ratio for samples grown with and without W-A at different surface deposition temperatures of 90 ℃ and 140

This article is protected by copyright. All rights reserved.

°C. The OSR is reported in the unit of part per millions (ppm) and reported electrical conductivity values belong to as-deposited samples with no additional acidic post-treatment steps.

Figure 2b shows that the in-plane σ is strongly dependent on OSR. At a given OSR value, the use of W-A growth enhances σ. The highest value of σ was achieved by utilizing W-A at a substrate temperature of 140 °C and an OSR value of 100 ppm. The resulting electrical conductivity of 7520 ± 240 S/cm is a new record for PEDOT in thin-film form and approaches the maximum σ value for a single-crystal nanowire (ca. 8797 ± 1178 S/cm).[27] It is noteworthy to mention that the record high electrical conductivity (7520 ± 240 S/cm) is achieved in PEDOT thin film with the thickness of 14 nm in a 2D conduction mechanism region (generally, region with the thickness less than 20 nm[28]), by optimizing the texture and nanostructure, which will be discussed further. As the $SbCl_5$ saturation ratio increases in films grown at 90 °C, the in-plane σ decreases. The same trend appears in films deposited at 140 °C, except at lowest OSR value (ca. 50 ppm).

Previously, an enhancement of σ was observed for methanol rinsing of oCVD PEDOT thin films grown using $FeCl_3$.[44] For the $FeCl_3$ solid oxidant, rinsing was hypothesized to remove low volatility oxidation byproducts such as $FeCl_2$. We hypothesis that the more volatile oxidant used here produces oxidation byproducts capable of directly desorbing from the growing surface, and thus, do not need to be rinsed away. The most common oxidant by-products as a result of $SbCl_5$ decomposition is $SbCl_3$. The vapor pressure of $SbCl_3$ is about 1 Torr at 49 °C[42], confirms that this oxidation by-product is volatile, making it possible to off-gas during the deposition and desorbs from the surface; thus, there is no need to remove it by rinsing. Indeed, rather than increase σ by rinsing, a 5 to 10% reduction in σ was observed after the methanol (MeOH) rinsing of the PEDOT grown using $SbCl_5$ (Table S3, Supporting Information), likely due to a small reduction in the Cl^- doping concentration. Avoiding the need for post-deposition rinsing makes the oCVD method a true single-step process, which is a great benefit of using volatile oxidants.[7]

Author Manuscript

This article is protected by copyright. All rights reserved.

Consistent with the hypothesis of volatile oxidation byproducts, the X-ray photoelectron spectroscopy (XPS) analyses of films grown at 140 ˚C (**Figure 3a**) reveals < 0.06 at. % antimony (Sb) for OSR of ≤190 ppm and ~0.52 at % Sb for an OSR of 290 ppm (Table S4, Supporting Information). Films grown with and without W-A at an OSR of 100 ppm display similar XPS survey spectra (Figure 3a) but differ in their high-resolution Cl 2p XPS spectra (Figure 3b,c). Assignments of the six component peaks in Figure 3b,c was made by analogy to $FeCl_3$-doped poly(3-alkyl-2,5-thienylene-alt-1,4-phenylene) ($PBTC_n$).[45] The two C-Cl peaks in Figure 3b,c are related to the chlorination of the conjugated backbone.[45] The lower concentration of the two C-Cl peaks in Figure 3c indicates a reduced degree of over-oxidation with W-A growth. The two ionic Cl peaks in Figure 3b,c are attributed to the $SbCl_6^-$ and Cl^-. While Cl^- is a well-known dopant in oCVD PEDOT, any ionic configuration of chlorine such as $SbCl_6^-$ that yields the hole carrier in the polymer chain can also be considered a dopant. The increased intensity of Cl^-peaks is consistent with the hypothesis of improved decomposition of the $SbCl_5$ oxidant in the presence of water.

The atomic force microscopy (AFM) was employed to clarify the impact of W-A growth on the surface morphology of PEDOT thin films. The height AFM images in Figure 3d-g show that the root mean square (rms) roughness of films is low (< 1.5 nm), as desired for integration into devices. The impact of W-A growth on surface roughness is more dominant than the effect of either growth temperature or OSR as can be observed in Figure 3d-g. The higher surface roughness of samples deposited with W-A than their counterparts deposited without water vapor might be attributed to the increase of crystallite size. At the uninterrupted vapor flow of reactants to the reactor, water continuously reacts with oxidant and results in better decomposition of $SbCl_5$ oxidant to Sb^+ and chloride (Cl^-). It is noteworthy to mention that polymerization follows the well-known step-growth mechanism,[1,2,39] and the presence of water vapor yields a better decomposition of oxidant to water solvated ionic products, such as Cl^-. Based on the solubility characteristic of $SbCl_5$ in water and the proton scavenger characteristic of water vapor, the formation of hydronium ions (H_3O^+) is expected. We hypothesize that easier accessibility of EDOT monomer to Cl^- in the W-A growth results in the formation of crystallites with the larger size. The presence of backbone chlorination (C-Cl peaks) and

This article is protected by copyright. All rights reserved.

Author Manuscript

$SbCl_6^-$ dopant would possibly disrupt the crystallinity. As demonstrated by HR-XPS (Figure 3b,c), the W-A growth yields a higher amount of Cl^- dopant than the backbone chlorination and $SbCl_6^-$ dopant, thus yields better crystallinity. In addition to the better decomposition of oxidant, it is reported that water vapor acts as a proton scavenger which yields the repetition of the step-growth polymerization cycle.[46,47] The oxidation of EDOT monomers to form dimers releases protons. When water is present, the protons can be scavenged to form the H_3O^+. By reducing the concentration of protons, the equilibrium of EDOT oxidation shifts towards the dimer product. Protons are also released as the dimers are oxidized to tetramers, and as the step-growth cycle repeats, pairs of n-mers form a 2n-mers. Thus, the ability of water to scavenge protons favors the formation of higher molecular weight PEDOT chains.

Author Manuscript

This article is protected by copyright. All rights reserved.

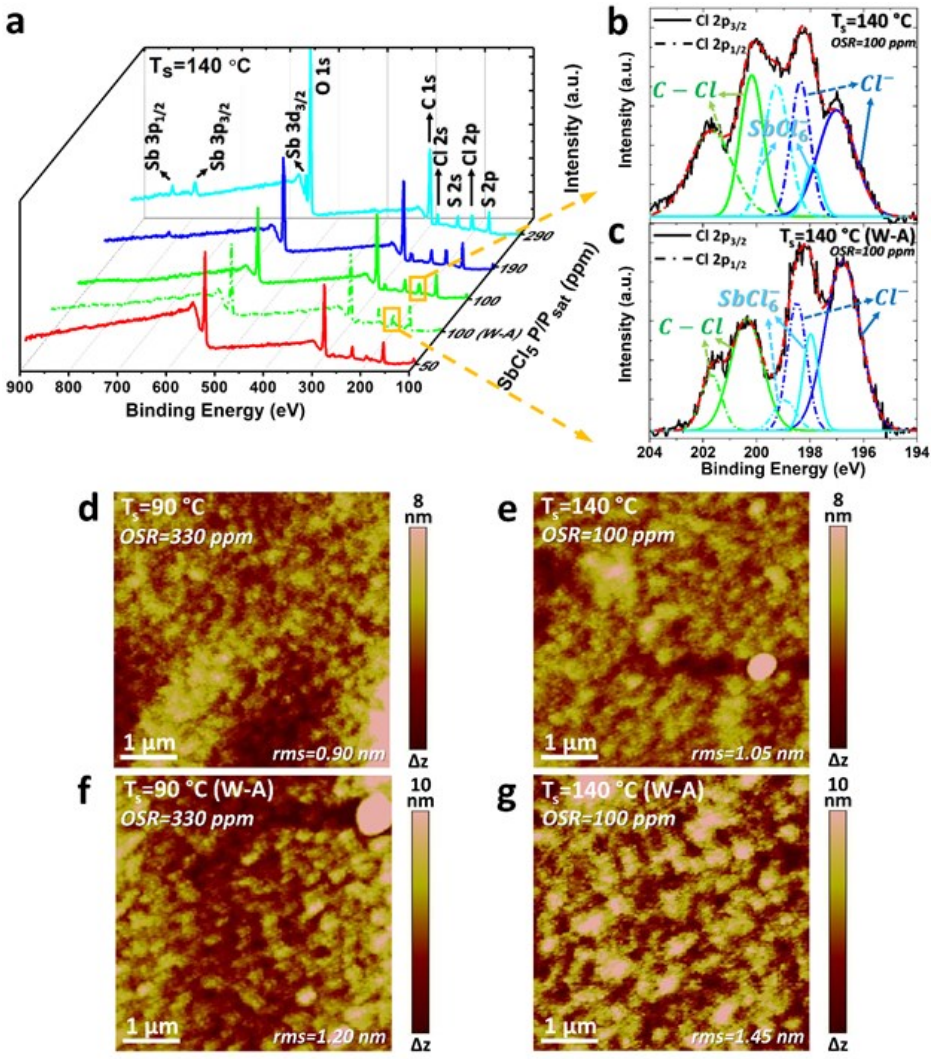

Figure 3. Stoichiometry and surface morphology of PEDOT thin films. a) Survey XPS scans of as-deposited PEDOT thin films grown with and without W-A at 140 ˚C at various OSR. XPS core-level high-resolution spectra of Cl 2p, for b) without W-A and c) with W-A in films deposited at 140 ˚C and OSR value of 100 ppm. d-g) The height AFM images of as-deposited samples grown with and without W-A at different surface deposition temperatures. At the fixed OSR value, the deposited samples with W-A exhibit higher surface roughness than their counterparts grown without using water vapor.

Figure 4a exhibits the normalized attenuated total reflection-Fourier transform infrared (ATR-FTIR) spectrum. In the spectrum of all six films, the absence of C_α-H stretching band at 754 cm^{-1} and the presence of the expected vibrational modes for the thiophene and ethylenedioxy rings confirms the successful polymerization of the intact EDOT monomer units. The intensity of C-O vibration peak at ~1050 cm^{-1} decreases by an increase of OSR in both deposition temperature, as shown in Figure 4a. Such behavior is attributed to the over-oxidation and degradation of ethylenedioxy ring in high OSR

Author

This article is protected by copyright. All rights reserved.

value (e.g., > 290 ppm). It is noteworthy that the C-O vibration peak of PEDOT grown with W-A is relatively sharper and exhibits higher intensity than its counterparts deposited without W-A. The presence of a quinoid structure, that is related to the C=C asymmetric stretching vibration at ~1520 cm^{-1}, can be noted in all samples. However, at the deposition temperature of 90 °C the appearance of a new peak with low intensity at ~1460 cm^{-1} is observed, which is related to the existence of slightly benzoid structure.

The Raman spectrum (Figure 4b) shows that increased growth temperature narrows the symmetric C_α=C_β stretching vibration and induces redshift to the lower wavenumber by ~15 cm^{-1}. For growth at 140°C, small redshifts are also observed with increasing OSR and use of W-A (Figure S2, Supporting Information). The redshift of the symmetric C_α=C_β stretching vibration indicates a higher fraction of quinoid structure. A change from benzoid to quinoid local bonding structure (Figure 4c) corresponds to the polymer chain transforming from a coil to a linear conformation. The linear conformation associated with the quinoid structure is favorable for enhancing interchain interaction and thereby enhancing σ.[48] The quinoid structure yields the rise in the double-bond character of the thiophene inter-ring and induces the better molecular ordering due to the suppression of chain distortion and lowering the bond length alternation (BLA).[49–51] As the outcome of obtaining a quinoid structure, the increase of interchain interaction can be expected due to increased planarity. Using W-A growth at 140°C produces a small redshift at OSR values of 50, 100, and 150 ppm (Figure S2, Supporting Information). Thus, it can be concluded that utilizing water vapor leads to an increase the linear arrangement of polymer chains, possibly because of lower levels of backbone chlorination, as detected by XPS.

Author Manuscript

This article is protected by copyright. All rights reserved.

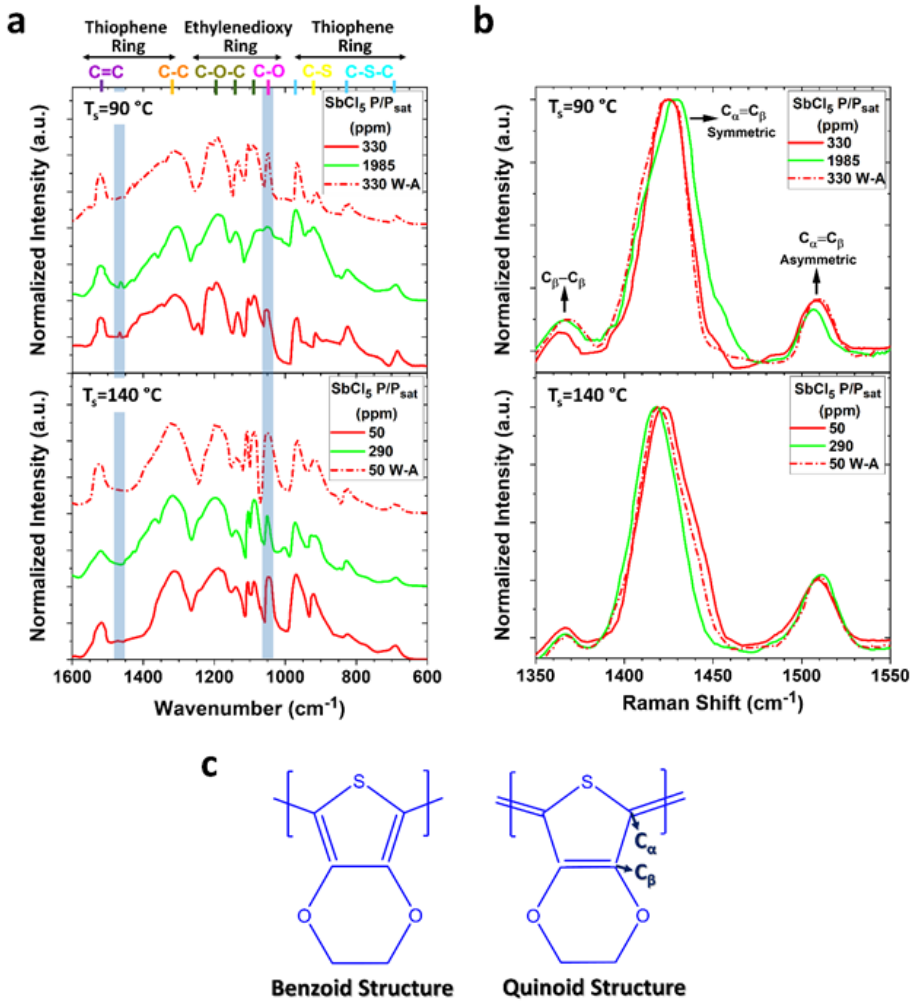

Figure 4. Impact of $SbCl_5$ saturation ratio and W-A on the PEDOT polymerization. a) FTIR spectra of as-deposited PEDOT thin films grown with and without W-A at various OSR and deposition temperatures. b) Typical Raman spectra of as-deposited samples grown with and without W-A at different deposition temperatures and OSR values. c) Benzoid and quinoid molecular structures of PEDOT.

The Grazing incidence X-ray diffraction (GIXRD) shows the predominance of the (020) peak corresponding to the face-on texture in the semicrystalline PEDOT films (**Figure 5**a,b). In samples grown at 90 ˚C at OSR values >1320 ppm (Figure 5a), the appearance of the (100) peak indicates that the film texture is a mixed orientation of face-on and edge-on. The lower OSR in films grown at 90 ˚C (Figure 5a) and all the films grown at 140 ˚C (Figure 5b) show only the (020) peak, characteristic of highly face-on texture. Generally, the PEDOT chains have sufficient ability to reorient at temperatures above glass transition (T_g),[1,6] which is ~100 ˚C for PEDOT, as illustrated in Figure 1b. Crystallites do

This article is protected by copyright. All rights reserved.

not necessarily deposit in their equilibrium configuration. For substrate temperatures lower than T_g, the crystallite remains kinetically trapped in its non-equilibrium state. When the surface temperature exceeds T_g, the crystallite can reorient to minimize its interfacial energy between the substrate and one face of the PEDOT crystallite. This behavior would be analogous to the impact of surface energy on the orientation of block copolymers in directed self-assembly.[52]

For optimizing in-plane σ, a high degree of face-on orientation is a more desirable than a mix of face-on and edge-on orientations because of lower energy barrier of intercrystallite charge transport.[1,6,7,29] The mixed face-on and edge-on orientation deteriorates the percolation pathway and results in a low σ.[6] It is noteworthy to emphasize that high electrical conductivity can be achieved in both highly face-on or highly edge-on orientation, since the conjugated backbone (pathway with high mobility of charge carrier) is located in the plane of thin-film in both orientations. In general, the charge transport between two adjacent crystallites with the same orientation is easier than between crystallites of different orientations. When adjacent crystallites have the same orientation, the polymer tie-chains with the conductive linear configuration can extend between the two crystallites. In contrast, for adjacent crystallites with a different orientation, tie-chains must adopt nonlinear configurations which are not electrically conductive, thus deteriorating the percolation pathway. The schematic illustration regarding electrical conductivity enhancement by alternating mixed-orientation to highly face-on orientation is exhibited in Figure 1b. Generally, the orientation of semi-crystalline conjugated polymers is strongly influenced by the fabrication method, size of introduced counter-ion dopant, and process parameters.[6] Similar to Figure 1b, the same behavior of increasing the electrical conductivity by changing the orientation from the mixed to the highly edge-on can be expected.

Average crystallite sizes were extracted from the GIXRD using the Scherrer equation[53] (Table S5, Supporting Information). For all films grown without W-A, the average size of the face-on and edge-on crystallites was ~3.2 nm and ~6.7 nm, respectively. Crystallite size increased ~18% with W-A (as illustrated in Figure 1a), potentially due to the better accessibility of EDOT monomer to the counter-ion dopant, which is well matched with the AFM results (Figure 3d-g). The use of W-A limits

This article is protected by copyright. All rights reserved.

Author Manuscript

the oxidation and thus reduces the concentration of chlorinated defects on the polymer chain backbone, as demonstrated in Figure 3b,c. The less defected chains resulting from W-A growth assemble more readily into the large crystallites. The overall charge transfer rate, k_{total}, across N face-on oriented crystallites at a specific charge transfer rate (k), is given by:[7]

$$k_{total} \sim \frac{k}{N} \qquad (2)$$

The use of W-A growth increases crystallite size (Table S5, Supporting Information), lowering the number of crystallites, N, across a given span, resulting in an increase in k_{total}, thus yields the σ enhancement.

Author Manuscript

This article is protected by copyright. All rights reserved.

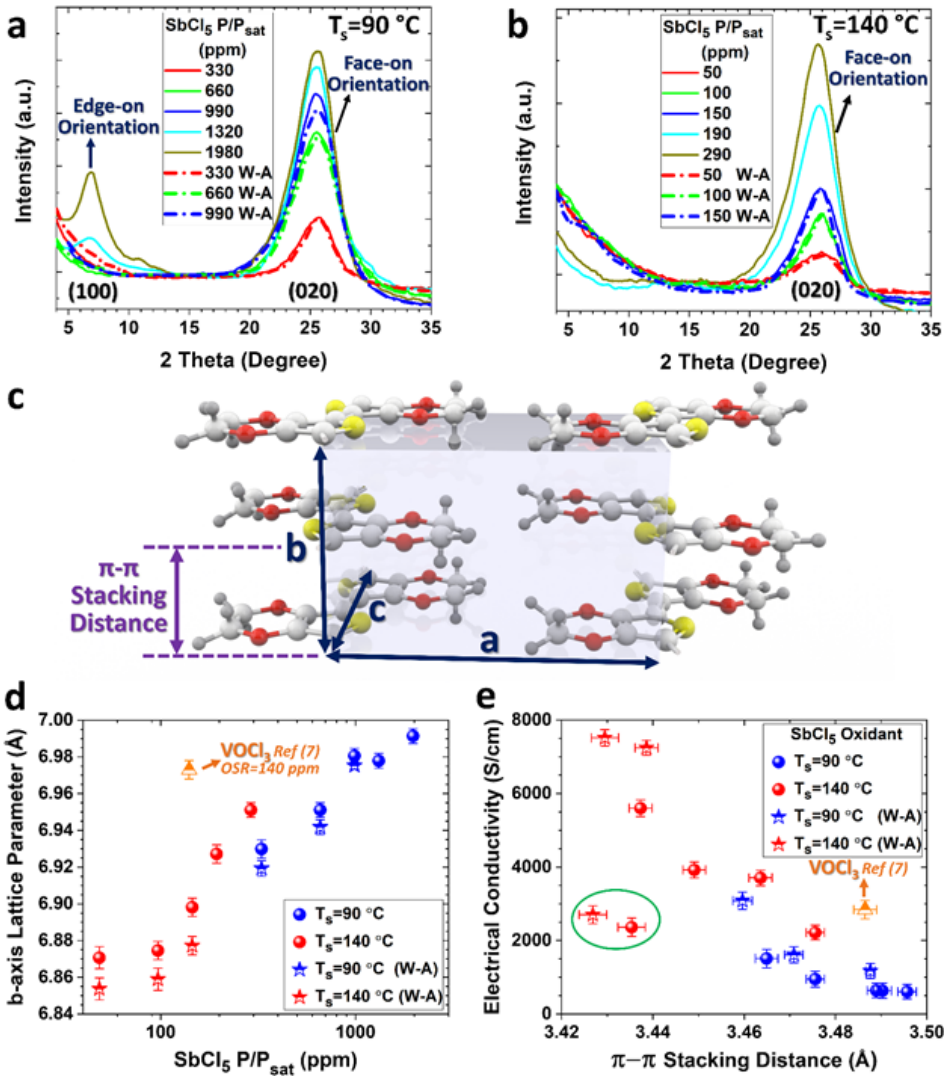

Figure 5. Impact of PEDOT texture and π-π stacking distance on the electrical conductivity. GIXRD patterns of as-deposited PEDOT thin films grown with and without W-A at various OSR and surface deposition temperature of a) 90 ˚C and b) 140 ˚C. c) Schematic illustration of orthorhombic unit cell of PEDOT as well as the lattice parameters and π-π stacking distance. d) Influence of OSR on the b-axis lattice parameter of samples grown at different conditions. e) Inverse trend of in-plane electrical conductivity and π-π stacking distance in as-deposited samples grown at different conditions. The data points inside the green circle are related to the films grown with the lowest OSR, which have the lowest incorporated doping level. The orange-color triangles in d) and e) exhibit the previously reported b-axis lattice parameter and electrical conductivity of as-deposited PEDOT thin films grown by $VOCl_3$ oxidant with the best performance.

Author

The π-π stacking distance in the orthorhombic structure of PEDOT (Figure 5c) is half of the b-axis lattice parameter. The GIXRD of (020) peak at high magnification (Figure S3, Supporting

This article is protected by copyright. All rights reserved.

Information) allows determination of the b-axis lattice parameter. As a consequence of increasing the $SbCl_5$ saturation ratio, the diffracted (020) peak gradually shifts toward lower diffraction angles, which is an indication of increasing the π-π stacking distance. Figure 5d shows that the b-axis lattice parameter increases as OSR increases and may reflect increased dopant levels or rise in backbone chlorination as revealed by XPS (Figure 3a). At the same value of OSR, the use of $SbCl_5$ leads to a lower π-π stacking distance than that of previously reported using $VOCl_3$ (Figure 5d). The larger π-π stacking distances obtained using $VOCl_3$ may reflect a larger concentration of oxidant byproducts and oxidation damage. Figure 5d also exhibits that at the fixed OSR for $SbCl_5$, PEDOT thin films grown with W-A exhibit the lower b-axis lattice parameter than samples deposited without water vapor (as illustrated in Figure 1c). The reduced b-axis lattice parameter for W-A growth than without W-A can be attributed to the improved rearrangement of PEDOT chains due to the better decomposition of $SbCl_5$ oxidant, a lower amount of non-ionized dopant, and avoiding chlorination of the backbone due to over oxidation, as demonstrated by XPS results (Figure 3b,c).

Consistent with the hypothesis of interchain transport being the rate-limiting process for electrical transport,[6] Figure 5e shows that low π-π stacking distances correlates to higher σ, except for the two points which are circled in green. These two outlier points at low OSR have lower doping levels, as demonstrated by XPS (Table S4, Supporting Information), and also may lack of polymer chains of sufficient length to form tie-chains between crystallite pairs. The direction with high mobility of charge carrier is located along the polymer backbone of tie-chains. Thus, tie-chains contribute significantly to the overall conductivity between crystallites. When intercrystallite conductivity is high, tie-chain will not be the rate-limiting step to charge transport, instead the interchain charge transport within a crystallite becomes an important factor and rate-limiting. For W-A growth, the maximum σ of 7520 ± 240 S/cm occurs at π-π stacking distance of 3.43 Å (Figure 5e). At a similar, but slightly larger π-π stacking distance of 3.44 Å, an optimum in σ of ~5602 ± 310 S/cm occurs for films grown without W-A. The magnitude of the interchain charge transport can be described by an overlap integral, where the value of integral increases as the π-π stacking distance decreases (Eqn. 1).

This article is protected by copyright. All rights reserved.

Author Manuscript

According to the Einstein equation, the charge carrier mobility (μ) is given by:[6,7,34]

$$\mu = \frac{eD}{k_B T} = \frac{e}{k_B T}\left(\frac{1}{2n}\sum_i d_{ij}^2 k_{ij} P_{ij}\right)$$
$$= \frac{e}{k_B T}\left(\frac{1}{2n}\sum_i d_{ij}^2 P_{ij}\left(\frac{{t_\perp}^2}{\hbar}\sqrt{\frac{\pi}{\lambda k_B T}}\, exp\left[-\frac{(\Delta E_{ij}+\lambda)^2}{4\lambda k_B T}\right]\right)\right) \quad (3)$$

where e is the elementary charge, D is the diffusion coefficient, k_B is the Boltzmann constant, T is the absolute temperature, n is the integer number, d_{ij} is the center to center mass distance between crystallite i and j, P_{ij} is the is the relative diffusion probability, and k_{ij} is the charge transfer rate, $\hbar$ is the reduced Planck constant, λ is the charge carrier reorganization, and ΔE_{ij} is the energy difference between initial and final states on nearby chains.

The charge transfer rate (k), thus carrier mobility, is proportional to the square of the interchain charge transfer integral ($t_\perp$), as can be noted in Eqn. 3. The change transfer integral grows exponentially with decreasing the π-π stacking distance between chains, thus carrier mobility and electrical conductivity increases exponentially. The interchain charge transfer integral is expected to be slightly higher in W-A growth due to the lower π-π stacking distance, which yields a higher charge transfer rate (increasing k). It is noteworthy to mention that the observed σ enhancement of ~1140% (~11.4-fold) in oCVD PEDOT thin film with the reduction of π-π stacking distance (from 3.50Å down to 3.43Å) is in agreement with other conjugated polymers such as oCVD PEDOT grown with $VOCl_3$ oxidant,[7] PEDOT:PSS,[9,54] and P3HT.[55] Generally, each 0.01 Å reduction in the π-π stacking distance of conjugated conducting and semiconducting polymers yields the substantial enhancement of σ, as a consequence of increase in the interchain charge transfer integral.[6]

Electrical conductivity is highly influenced by the π-π stacking distances, planarity of backbone, preferred orientation, crystallite size, and film thickness of conjugated polymers. In the situation of superior intercrystallite conductivity through tie-chains in a highly orientated face-on (or highly oriented edge-on), the interchain charge transport within a crystallite becomes a rate-limiting factor.

This article is protected by copyright. All rights reserved.

Author Manuscript

Thus, the reduction of π-π stacking distance plays a critical role in enhancing carrier mobility and electrical conductivity due to the exponential rise in the interchain charge transfer integral, as shown in Eq. 1 and Eq. 3. In such a scenario and considering that all other parameters are almost fixed, the ~11.4-fold improvement in the electrical conductivity due to the 0.07 Å reduction in the π-π stacking distance gives the wave function overlap decay length ($1/\gamma$) of ~0.05 Å. It is noteworthy to mention that in the case of highly face-on orientation (samples grown at 140 ˚C), the value of $1/\gamma$ is estimated to be ~0.08 Å due to the increase of electrical conductivity from 2220 to 7520 S/cm as a consequence of π-π stacking reduction from 3.48 Å to 3.43 Å.

The optical transmittance spectra of samples grown on the glass microscope slides (**Figure 6a**), which are obtained using ultraviolet-visible–near infrared (UV-vis–NIR) analyses, are exhibited in Figure S4 (Supporting Information). The extracted optical bandgap energy (E_g) values from the absorption spectra of samples (Figure S5, Supporting Information) correlate inversely with OSR. The reduction of E_g (from 3.30 down to 2.0 eV) as a consequence of increasing the OSR (from 50 to 1980 ppm) is associated with removing more electrons from the highest occupied molecular orbital (HOMO) and providing a more positively charged holes as charge carriers along the polymer backbone.[6,7] The obtained E_g values for oCVD PEDOT films grown with $VOCl_3$ oxidant were in the range of 2.9-2.6 eV.[7] The reduction of the lower limit of E_g with ~0.6 eV in the case of PEDOT film grown with W-A oCVD and use of $SbCl_5$ oxidant compared to the $VOCl_3$ oxidant can be attributed to the incorporation of more ionic dopant in the PEDOT film instead of overoxidation and chlorination of backbone. By comparing the optical transmittance values at 550 nm (Figure S4, Supporting Information) and E_g values (Figure 6b), it can be noted that PEDOT thin film with a wider E_g displays higher transmittance. It is noteworthy to mention that optoelectronic tunability characteristics of PEDOT thin film using OSR is highly beneficial in band alignment between different layers in photovoltaic devices.[2]

The Urbach energy (E_U) represents the amount of structural and energetic disorder and can be estimated from the absorption coefficient (Figure S6, Supporting Information). The E_U indicates the

This article is protected by copyright. All rights reserved.

amount of localized states in the energy band diagram and low E_U value is the sign of better structural order.[6] The E_U increases by the increase in OSR (Figure 6c). At the fixed OSR value, the films grown with W-A exhibit relatively lower E_U (higher morphological order) than their counterparts grown without W-A, due to the crystallinity enhancement. The highest in-plane σ of 7520 ± 240 S/cm is obtained in sample with a minimum E_U value of 205 meV (grown with W-A at 140 °C and OSR of 100 ppm), which further demonstrates the superior morphological order of that sample grown with W-A. Besides, the low obtained E_U value (ca. 205 meV) in oCVD PEDOT grown by W-A with the use of $SbCl_5$ oxidant indicates the better morphological order, thus superior σ, than PEDOT:PSS (E_U value of 3040 meV)[56] and oCVD PEDOT grown by $VOCl_3$ oxidant (E_U value of 704 meV).[7]

There is a drawback on the optical transmittance in high carrier density due to the absorption of light by charge carriers. The presence of trade-off between optical transmittance and sheet resistance is exhibited in Figure 6d. To evaluate the optoelectronic characteristics of TCEs, the figure of merit ($FoM = \sigma_{dc}/\sigma_{op}$, where σ_{dc} and σ_{op} are the DC and optical conductivity, respectively) is defined.[6,57] The benchmark indicator of commercial viability of TCEs (e.g., $FoM \sim 35$) is shown by the dashed-green line in Figure 6d. As can be noted, the majority of samples have the FoM value higher than 35. The highest $FoM \cong 94$ (sheet resistance of ~60 Ω and optical transmittance of ~93.7%) is obtained in sample grown with W-A at 140 °C with theand OSR value of 150 ppm. As compared to the high reported FoM value in oCVD PEDOT thin films grown by $VOCl_3$[7] and $FeCl_3$[44,58] oxidants (upward and downward triangles in Figure 6d), the use of $SbCl_5$ oxidant with the W-A growth enhances the FoM value by 1.9× and 6.7×, respectively. The optoelectronic characteristics of oCVD PEDOT films can be tuned by adjusting the OSR and deposition temperature. In contrast, in spun-cast PEDOT:PSS, adding different organic solvents and surfactants, such as dimethyl sulfoxide (DMSO), is an alternative path for tuning the optoelectronic characteristic. It is noteworthy to mention that the achieved $FoM \cong 94$ in this study is ~1.8× higher than the highest reported value of 53 in PEDOT:PSS obtained by adding 5 wt.% DMSO to spun-cast solution.[59]

This article is protected by copyright. All rights reserved.

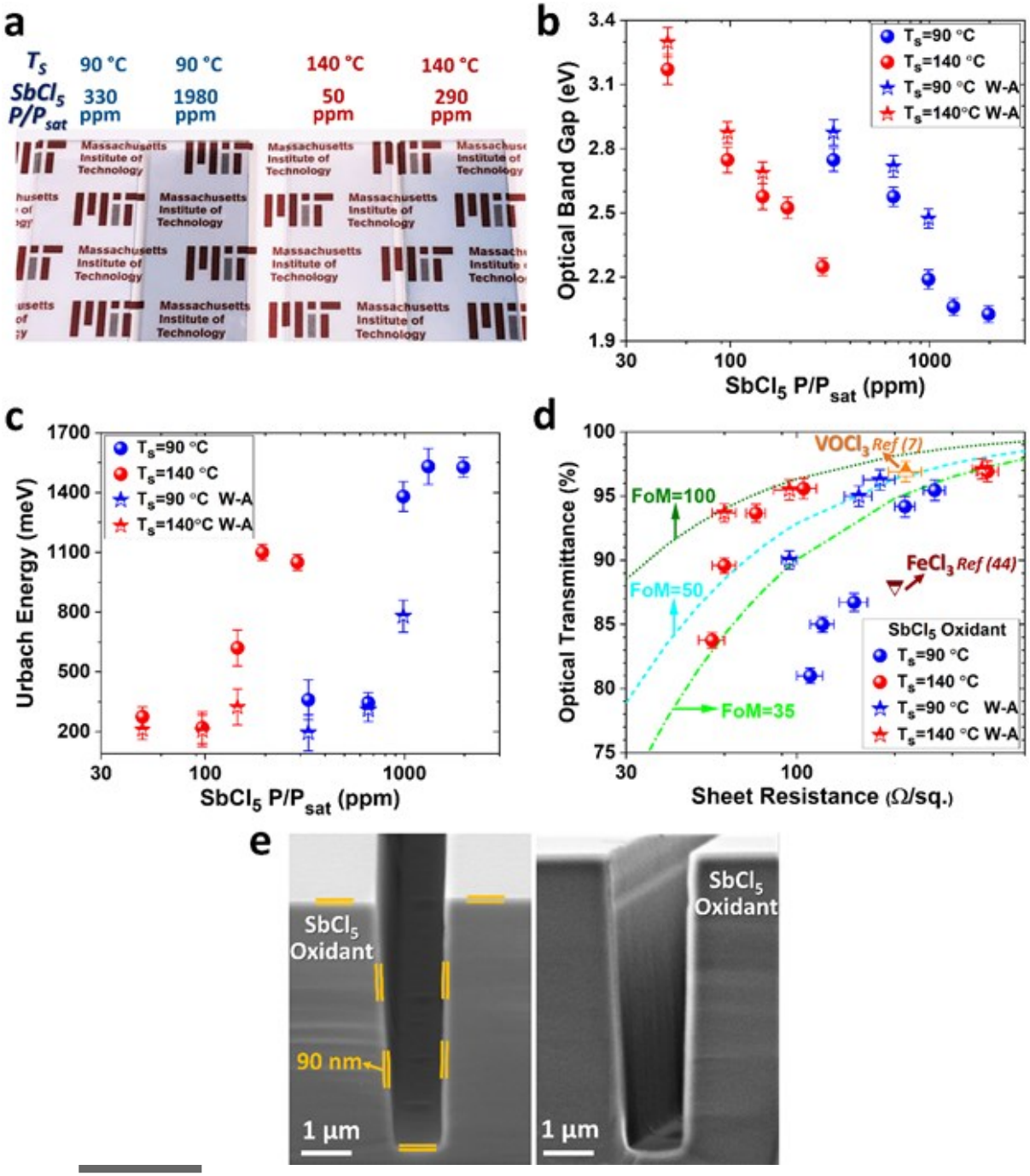

Figure 6. Optoelectronic characteristic of PEDOT thin films grown with the $SbCl_5$ oxidant. a) Photograph of PEDOT thin films grown at different OSR and temperatures on the microscope glass slides. b) Influence of OSR on the optical bandgap in samples grown at different conditions. c) Urbach energy values as a function of OSR in samples grown with and without W-A at different deposition temperatures. d) Optical transmittance and sheet resistance values of films grown at various conditions. e) Cross-sectional SEM image of sample grown by $SbCl_5$ oxidant on the silicon trench wafers with aspect ratio of ratio of ~11. Formation of highly conformal oCVD PEDOT thin film can be noted from different view angles, as shown in the right and left images.

This article is protected by copyright. All rights reserved.

The cross-sectional scanning electron microscopy (SEM) image demonstrates the ability of the oCVD method using $SbCl_5$ oxidant for growth of high conformality PEDOT thin film (Figure 6e). The cross-sectional SEM image of PEDOT thin film grown on a wider area of the trench silicon wafer is exhibited in Figure S7 (Supporting Information). While the oCVD method provides highly conformal and uniform PEDOT thin films, the spun-cast PEDOT:PSS does not exhibit such advantage,[2,40,60] due to the surface tension effects and formation of an air-gap, bridging, and meniscus.[1,40] Depositing ultrathin conformal oCVD PEDOT coating on high aspect ratio features yields significant advantages in many advanced technologies, including wearable electronics,[61] and electrochemical energy storage devices.[40,62]

3. Conclusion

In summary, these results indicate that the in-plane electrical conductivity of semicrystalline PEDOT thin films in the face-on orientation can be rate limited by interchain transport, resulting in an inverse correlation between the conductivity and π-π stacking distance. The high-record electrical conductivity of 7520±240 S/cm was achieved in as-deposited oCVD PEDOT thin films grown with W-A at the deposition temperature of 140 °C and OSR value of 100 ppm. The use of W-A growth provides a better decomposition of oxidant and induces a higher amount of Cl^- dopant instead of backbone chlorination and $SbCl_6^-$ dopant, which results in a high degree of perfection for PEDOT polymerization. As the outcome of less backbone chlorination and $SbCl_6^-$ dopant, the increased crystallite size and reduced π-π stacking distance is achieved in the W-A growth of PEDOT thin films using the oCVD method. In general, W-A oCVD method is a promising approach for the electrical conductivity enhancement as a consequence of (i) π-π stacking distance reduction, (ii) rise in crystallite size, (iii) increase of linear configuration of polymer chains (quinoid structure), (iv) reduction of the Urbach edge, and (v) reduction of non-ionized counter-ion dopant. The presence of tie-chains in highly face-on orientation contributes significantly to the overall conductivity between

This article is protected by copyright. All rights reserved.

Author Manuscript

crystallites. However, in the case of superior intercrystallite conductivity, the interchain charge transport within a crystallite becomes an important rate-limiting factor. The higher interchain charge transport, thus increased overall charge transfer rate, can be achieved by lowering the π-π stacking distance through engineering the dopant level and OSR. In addition, the increased crystallite size is another parameter that yields a higher overall charge transfer rate due to the reduced numbers of crystallites that need to be connected by tie-chains. This study reveals an important milestone in enhancing the electrical conductivity of as-deposited PEDOT thin film without the need for acidic post-deposition step through systematic tuning of OSR in the W-A oCVD method.

4. Experimental Section

The EDOT monomer (purchased from Sigma-Aldrich, 97% purity) and $SbCl_5$ oxidant (purchased from Sigma-Aldrich, 99% purity) were used as received without further purification. The EDOT and $SbCl_5$ were heated in a temperature-controlled glass jar at the temperature of 140 and 65 °C, respectively. The deionized (DI) water kept in a bubbler at room temperature, and the carrier gas of argon was used to deliver the DI water vapor to the reactor. The pressure of reactor was maintained at a fixed value of 150 mTorr. The detailed information relates to transferring the flow rate to SCCM is provided in Supporting Information and the processing information is provided in Table S1 (Supporting Information).

Materials characterization is performed on as-deposited PEDOT thin films without any acidic rinsing post-treatments. The sheet resistance (R_s) was recorded with a standard four-point probe set-up using a Jandal four-point probe (CYL-1.0-100-TC-100-RM3) connected to Keithley 2000 and 2400 multimeter. The electrical conductivity was extracted from the equation ($\sigma = \frac{1}{(R_s t)}$, where σ is the electrical conductivity (Siemens/cm, S/cm), R_s is the sheet resistance (Ω), and t is the film thickness (nm). The film thickness was measured by a step-height profilometer (Veeco Dektak 150) and

This article is protected by copyright. All rights reserved.

Author Manuscript

confirmed with the Atomic Force Microscope (AFM, Veeco Dimension 3100). Grazing incidence X-ray diffraction (GIXRD) measurements were carried out using a Rigaku Smart lab diffractometer equipped with a Cu-K_α radiation of λ=0.15418 nm. Scanning electron microscopy (SEM) was carried out using a cold field-emission gun Scanning electron microscope (FEG-SEM), JEOL 6700F. X-ray photoelectron spectroscopy (XPS) samples were analyzed using a Surface Science Instruments SSX-100 with an operating pressure of approximately 2×10^{-9} Torr and the monochromatic Al K_α radiation. In XPS measurement, the binding energy (BE) was extracted by subtracting the X-ray energy (here 1486.70 eV) from the electron kinetic energy and stoichiometry values were extracted using CasaXPS software. Attenuated total reflection-Fourier transform infrared (ATR-FTIR) spectra were collected using a NICOLET iS50 FT-IR with ATR attachment. Raman spectroscopy analyses were performed by a Horiba Jobin-Yvon HR800 with a laser wavelength of 785 nm. Ultraviolet-visible-near infrared (UV-vis-NIR) spectroscopy was carried out using a Cary 7000 Universal Measurement Spectrometer equipped with an integrating sphere detector. The figure of merit ($FoM = \sigma_{dc}/\sigma_{op}$) values are extracted from $T(\lambda) = \left(1 + \frac{Z_0}{2R_{sh}}\frac{\sigma_{op}}{\sigma_{dc}}\right)^{-2}$, where $T(\lambda)$ is the transmittance at λ = 550 nm, $Z_0 = 377\ \Omega$ (impedance of free space), and R_{sh} is the sheet resistance ($\Omega\ sq^{-1}$)[6,57].

Author Manuscript

Author contributions:

M.H: Fabrication, Conceptualization, Methodology, Validation, Formal analysis, Investigation, Data Curation, Writing – Original Draft, Writing – Review & Editing, Visualization. **M.T.R:** Conceptualization, Methodology. **E.F.G:** Conceptualization, Methodology. **K.K.G:**

This article is protected by copyright. All rights reserved.

Conceptualization, Methodology, Validation, Writing – Original Draft, Writing – Review & Editing, Visualization, Supervision.

Competing interests:

Authors declare no competing interests.

Author Manuscript

References

[1] K. K. Gleason, *Nat. Rev. Phys.* **2020**, *2*, 347.

[2] M. Heydari Gharahcheshmeh, K. K. Gleason, *Adv. Mater. Interfaces* **2019**, *6*, 1.

[3] S. Kaviani, M. Mohammadi Ghaleni, E. Tavakoli, S. Nejati, *ACS Appl. Polym. Mater.* **2019**, *1*, 552.

[4] H. Chen, C. Li, *Chinese J. Polym. Sci.* **2020**, *38*, 435.

[5] L. Krieg, F. Meierhofer, S. Gorny, S. Leis, D. Splith, Z. Zhang, H. von Wenckstern, M. Grundmann, X. Wang, J. Hartmann, C. Margenfeld, I. M. Clavero, A. Avramescu, T. Schimpke, D. Scholz, H.-J. Lugauer, M. Strassburg, J. Jungclaus, S. Bornemann, H. Spende, A. Waag, K. Gleason, T. Voss, *Nat. Commun.* **2020**, *11*, 5092.

[6] M. Heydari Gharahcheshmeh, K. K. Gleason, *Mater. Today Adv.* **2020**, *8*, 100086.

[7] M. Heydari Gharahcheshmeh, M. M. Tavakoli, E. F. Gleason, M. T. Robinson, J. Kong, K. K. Gleason, *Sci. Adv.* **2019**, *5*, eaay0414.

[8] L. Bießmann, N. Saxena, N. Hohn, M. A. Hossain, J. G. C. Veinot, P. Müller-Buschbaum, *Adv. Electron. Mater.* **2019**, *5*, 1800654.

[9] S. Kee, N. Kim, B. S. Kim, S. Park, Y. H. Jang, S. H. Lee, J. Kim, J. Kim, S. Kwon, K. Lee, *Adv. Mater.* **2016**, *28*, 8625.

[10] S. Macher, M. Schott, M. Sassi, I. Facchinetti, R. Ruffo, G. Patriarca, L. Beverina, U. Posset, G. A. Giffin, P. Löbmann, *Adv. Funct. Mater.* **2020**, *30*, 1906254.

[11] P. Yadav, S. Naqvi, A. Patra, *RSC Adv.* **2020**, *10*, 12395.

[12] J. P. S. A. Schultheiss, M. Gueye, A. Carella, A. Benayad, S. Pouget, J. Faure-Vincent, R. Demadrille, A. Revaux, *ACS Appl. Polym. Mater.* **2020**, *2*, 2686.

[13] K. H. Hong, K. W. Oh, T. J. Kang, *J. Appl. Polym. Sci.* **2005**, *97*, 1326.

[14] I. Petsagkourakis, E. Pavlopoulou, G. Portale, B. A. Kuropatwa, S. Dilhaire, G. Fleury, G. Hadziioannou, *Sci. Rep.* **2016**, *6*, 30501.

This article is protected by copyright. All rights reserved.

[15] M. N. Gueye, A. Carella, N. Massonnet, E. Yvenou, S. Brenet, J. Faure-Vincent, S. Pouget, F. Rieutord, H. Okuno, A. Benayad, R. Demadrille, J. P. Simonato, *Chem. Mater.* **2016**, *28*, 3462.

[16] L. Shen, P. Liu, C. Liu, Q. Jiang, J. Xu, X. Duan, Y. Du, F. Jiang, *ACS Appl. Polym. Mater.* **2020**, *2*, 376.

[17] R. Brooke, P. Cottis, P. Talemi, M. Fabretto, P. Murphy, D. Evans, *Prog. Mater. Sci.* **2017**, *86*, 127.

[18] Y. Jia, L. Shen, J. Liu, W. Zhou, Y. Du, J. Xu, C. Liu, G. Zhang, Z. Zhang, F. Jiang, *J. Mater. Chem. C* **2019**, *7*, 3496.

[19] B. Li, K. H. Skorenko, H. Qiu, M. Mativetsky, D. B. Dwyer, W. E. Bernier, W. E. Jones, *Synth. Met.* **2020**, *260*, 116293.

[20] D. Bilger, S. Z. Homayounfar, T. L. Andrew, *J. Mater. Chem. C* **2019**, *7*, 7159.

[21] G. Bengasi, K. Baba, O. Back, G. Frache, K. Heinze, N. D. Boscher, *Chem. - A Eur. J.* **2019**, *25*, 8313.

[22] G. Bengasi, J. S. Desport, K. Baba, J. P. Cosas Fernandes, O. De Castro, N. D. Boscher, G. G. Bengasi, K. Heinze, *RSC Adv.* **2020**, *10*, 7048.

[23] M. Mirabedin, H. Vergnes, N. Caussé, C. Vahlas, B. Caussat, *Synth. Met.* **2020**, *266*, 116419.

[24] L. Krieg, Z. Zhang, D. Splith, H. von Wenckstern, M. Grundmann, X. Wang, K. K. Gleason, T. Voss, *Nano Express* **2020**, *1*, 010013.

[25] M. M. Tavakoli, M. Heydari Gharahcheshmeh, N. Moody, M. G. Bawendi, K. K. Gleason, J. Kong, *Adv. Mater. Interfaces* **2020**, 2000498.

[26] X. Li, A. Rafie, Y. Y. Smolin, S. Simotwo, V. Kalra, K. K. S. Lau, *Chem. Eng. Sci.* **2019**, *194*, 156.

[27] B. Cho, K. S. Park, J. Baek, H. S. Oh, Y. E. Koo Lee, M. M. Sung, *Nano Lett.* **2014**, *14*, 3321.

[28] A. Ugur, F. Katmis, M. Li, L. Wu, Y. Zhu, K. K. Varanasi, K. K. Gleason, *Adv. Mater.* **2015**, *27*, 4604.

[29] X. Wang, X. Zhang, L. Sun, D. Lee, S. Lee, M. Wang, J. Zhao, Y. Shao-Horn, M. Dincă, T. Palacios, K. K. Gleason, *Sci. Adv.* **2018**, *4*, eaat5780.

[30] P. Kovacik, G. Del Hierro, W. Livernois, K. K. Gleason, *Mater. Horizons* **2015**, *2*, 221.

[31] M. C. Barr, J. A. Rowehl, R. R. Lunt, J. Xu, A. Wang, C. M. Boyce, S. G. Im, V. Bulović, K. K. Gleason, *Adv. Mater.* **2011**, *23*, 3500.

[32] J. J. Kim, L. K. Allison, T. L. Andrew, *Sci. Adv.* **2019**, *5*.

[33] L. Sun, G. Yuan, L. Gao, J. E. Yang, M. Chhowalla, M. Heydari Gharahcheshmeh, K. K. Gleason, Y. S. Choi, B. H. Hong, Z. Liu, *Nat. Rev. Methods Prim.* **2020**, *In Press*.

[34] V. Coropceanu, J. Cornil, D. A. da Silva Filho, Y. Olivier, R. Silbey, J. L. Brédas, *Chem. Rev.* **2007**, *107*, 926.

[35] S. Ko, E. T. Hoke, L. Pandey, S. Hong, R. Mondal, C. Risko, Y. Yi, R. Noriega, M. D.

This article is protected by copyright. All rights reserved.

Author Manuscript

McGehee, J. L. Brédas, A. Salleo, Z. Bao, *J. Am. Chem. Soc.* **2012**, *134*, 5222.

[36] M. S. Chen, J. R. Niskala, D. A. Unruh, C. K. Chu, O. P. Lee, J. M. J. Fréchet, *Chem. Mater.* **2013**, *25*, 4088.

[37] S. Wei, L. P. Ma, M. L. Chen, Z. Liu, W. Ma, D. M. Sun, H. M. Cheng, W. Ren, *Carbon N. Y.* **2019**, *148*, 241.

[38] J. M. Feng, Y. J. Dai, *Nanoscale* **2013**, *5*, 4422.

[39] K. K. Gleason, *J. Vac. Sci. Technol. A* **2020**, *38*, 020801.

[40] M. Heydari Gharahcheshmeh, C. Tai-Chieh Wan, Y. A. Gandomi, K. Greco, A. Forner-Cuenca, Y. M. Chiang, F. R. Brushett, K. K. Gleason, *Adv. Mater. Interfaces* **2020**, *2000855*.

[41] P. Moni, J. Lau, A. C. Mohr, T. C. Lin, S. H. Tolbert, B. Dunn, K. K. Gleason, *ACS Appl. Energy Mater.* **2018**, *1*, 7093.

[42] PubChem. *https://pubchem.ncbi.nlm.nih.gov/*.

[43] S. Nejati, T. E. Minford, Y. Y. Smolin, K. K. S. Lau, *ACS Nano* **2014**, *8*, 5413.

[44] R. M. Howden, E. D. McVay, K. K. Gleason, *J. Mater. Chem. A* **2013**, *1*, 1334.

[45] S. C. Ng, J. M. Xu, H. S. O. Chan, *Macromolecules* **2000**, *33*, 7349.

[46] H. Goktas, X. Wang, A. Ugur, K. K. Gleason, *Macromol. Rapid Commun.* **2015**, *36*, 1283.

[47] M. Fabretto, K. Zuber, C. Hall, P. Murphy, *Macromol. Rapid Commun.* **2008**, *29*, 1403.

[48] J. Ouyang, Q. Xu, C. W. Chu, Y. Yang, G. Li, J. Shinar, *Polymer (Guildf).* **2004**, *45*, 8443.

[49] Y. D. Park, D. H. Kim, J. A. Lim, J. H. Cho, Y. Jang, W. H. Lee, J. H. Park, K. Cho, *J. Phys. Chem. C* **2008**, 1705.

[50] O. T. Prior, F. Formation, R. Polyalkylthiophenes, *Adv. Mater.* **2000**, 1594.

[51] Y. Cheng, S. Yang, C. Hsu, *Chem. Rev* **2009**, *109*, 5868.

[52] P. Moni, H. S. Suh, M. Dolejsi, D. H. Kim, A. C. Mohr, P. F. Nealey, K. K. Gleason, *Langmuir* **2018**, *34*, 4494.

[53] B. D. Cullity, *Elements of X-Ray Diffraction*; Addison-Wesley: London, 1978.

[54] C. M. Palumbiny, F. Liu, T. P. Russell, A. Hexemer, C. Wang, P. Müller-buschbaum, *Adv. Mater.* **2015**, *27*, 3391.

[55] V. Vijayakumar, Y. Zhong, V. Untilova, M. Bahri, L. Herrmann, L. Biniek, N. Leclerc, M. Brinkmann, *Adv. Energy Mater.* **2019**, *9*, 1900266.

[56] J. Ram, R. G. Singh, F. Singh, V. Kumar, V. Chauhan, R. Gupta, U. Kumar, B. C. Yadav, R. Kumar, *J. Mater. Sci. Mater. Electron.* **2019**, *30*, 13593.

[57] V. Scardaci, R. Coull, J. N. Coleman, *Appl. Phys. Lett.* **2010**, *97*, 023114.

[58] S. Lee, D. C. Paine, K. K. Gleason, *Adv. Funct. Mater.* **2014**, *24*, 7187.

[59] E. Dauzon, A. E. Mansour, M. R. Niazi, R. Munir, D. Smilgies, X. Sallenave, C. Plesse, F.

This article is protected by copyright. All rights reserved.

Author Manuscript

Goubard, A. Amassian, *ACS Appl. Mater. Interfaces* **2019**, *11*, 17570.

[60] S. G. Im, D. Kusters, W. Choi, S. H. Baxamusa, M. C. M. van de Sanden, K. K. Gleason, *ACS Nano* **2008**, *2*, 1959.

[61] T. L. Andrew, L. Zhang, N. Cheng, M. Baima, J. J. Kim, L. Allison, S. Hoxie, *Acc. Chem. Res.* **2018**, *51*, 850.

[62] G. L. Xu, Q. Liu, K. K. S. Lau, Y. Liu, X. Liu, H. Gao, X. Zhou, M. Zhuang, Y. Ren, J. Li, M. Shao, M. Ouyang, F. Pan, Z. Chen, K. Amine, G. Chen, *Nat. Energy* **2019**, *4*, 484.

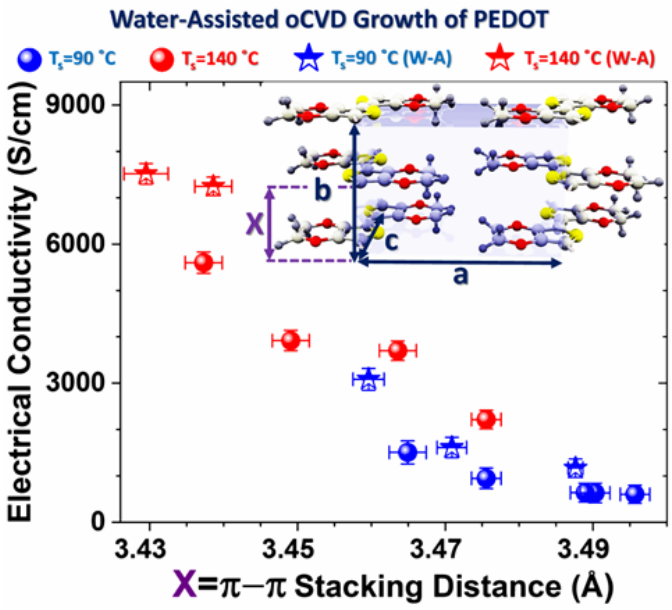

In poly(3,4-ethylenedioxythiophene) (PEDOT) thin films with a highly face-on orientation, the charge transport between chains within a crystallite becomes a rate-limiting factor, which is highly sensitive to the π-π stacking distance. Engineering π-π stacking distance in PEDOT films grown by water-assisted oxidative chemical vapor deposition (oCVD) yields a record high electrical conductivity of 7520 ± 240 S/cm.

Author Manuscript

This article is protected by copyright. All rights reserved.